Journal of Chemical and Pharmaceutical Sciences-JCHPS (2025) 18 (2): 67-81
Online ISSN: Online 2349-8552, Print ISSN: 0974-2115
Research Article | Pharmaceutical Sciences | MCI Approved | Peer-Reviewed | Refereed| OA Journal |

Design, Formulation and evaluation of Bicalutamide nanosponge using BOX-Behnken Design

Srinivas Pooduri*, Seema Tomar[1] and M. Srinivas Reddy[2]

***Research Scholar, Faculty of Pharmaceutical Sciences, Motherhood University, Dehradun Road, Karoundi village, Bhagwanpur post, Roorkee Tehsil, Haridwar Distt., Uttarakhand, India 247661.**

[1]Professor, Faculty of Pharmaceutical Sciences, Motherhood University, Dehradun Road, Karoundi village, Bhagwanpur post, Roorkee Tehsil, Haridwar Distt., Uttarakhand, India 247661.

[2]Professor, Beside L.M.D Police Station, Ramakrishna Colony, Thimmapur, Karimnagar, Telangana State, India-505527

Received: 29 Jan 2025 / Accepted: 20 Mar 2025 / Published online: 01 Apr 2025
*Corresponding Author Email: **srinuvas004@gmail.com**

ABSTRACT

One of the most common non-steroidal antiandrogens used to treat prostate cancer is biicalutamide, or BCL. Its therapeutic potential is severely hampered, nonetheless, by its poor solubility in water and its low oral bioavailability. The current research sought to create a bicalutamide sustained-release nanosponge (NS) medication delivery system that utilized β-cyclodextrin as a polymeric carrier. The formulation was then optimized using the Box-Behnken Design (BBD) inside a Quality by Design (QbD) framework. The solvent evaporation method was employed to prepare nanosponges, which were cross-linked using dimethyl carbonate. The optimal particle size, entrapment efficiency, and drug release behavior were achieved by methodically optimizing key formulation factors such as polymer concentration, cross-linker quantity, and stirring time. The optimized nanosponge sample had an entrapment effectiveness of 82.49 ± 0.36%, a particle size of 176.35 ± 2.06 nm, and a polydispersity index (PDI) of 0.273 ± 0.43. The drug was released at a rate of around 90.45 ± 0.29% over the course of 24 hours, according to in vitro release experiments, indicating a sustained release profile. A first-order model was followed by the release kinetics, suggesting that the release mechanism was concentration dependent. Imaging microscopy and transmission electron microscopy verified the nanosponges' porosity and spherical shape. Pharmacokinetic tests in rats showed that bicalutamide had a much longer half-life and much higher oral bioavailability when administered via the nanosponge system as opposed to the pure drug. Finally, the BCL-loaded nanosponges show promise as a delivery method for enhancing bicalutamide's solubility, bioavailability, and sustained release, which could have positive effects on prostate cancer treatment.

KEY WORDS: Bicalutamide; Pharmacokinetic; Box-Behnken Design; Quality by Design; Pharmacokinetic; Non-steroidal antiandrogen;

INTRODUCTION:

Rossi B. describe CDNS as intriguing cross-linked polymers. Their nanosized hydrophilic and lipophilic gaps effectively contain guest compounds in three dimensions. Activated carbonyl compounds (triphosgene, diphenyl carbonate, dimethyl carbonate, or organic dianhydrides) and cyclodextrins crosslink novel nanoporous materials [1]. Crupi V et al. describe the three-dimensional CD unit network approach. This network's hydrophobic and hydrophilic nanoparticles may encapsulate, transport, and selectively release inorganic and biological molecules. Cyclodextrin nanosponges are

Journal of Chemical and Pharmaceutical Sciences

Journal of Chemical and Pharmaceutical Sciences-JCHPS (2025) 18 (2): 67-81
Online ISSN: Online 2349-8552, Print ISSN: 0974-2115
Research Article | Pharmaceutical Sciences | MCI Approved | Peer-Reviewed | Refereed| OA Journal |

spherical scaffolds containing numerous medicinal molecule pockets, according to Selvamuthukumar. Pharmaceutics, biomedicine, cosmetics, bioremediation, water purification, catalysis, and agro-chemistry employ nanosponges to improve cyclodextrin performance [2]. Rossi B. et al. describe CDNS as intriguing cross-linked polymers. Their nanosized hydrophilic and lipophilic gaps effectively contain guest compounds in three dimensions. Acids, activated carbonyl compounds (triphosgene, diphenyl, dimethyl, or organic dianhydrides), and cyclodextrins crosslink new nanoporous materials. Crupi V et al. explain the method and three-dimensional CD unit network. This network's hydrophobic and hydrophilic nanoparticles may encapsulate, transport, and selectively release inorganic and biological molecules. Cyclodextrin nanosponges are spherical scaffolds containing numerous medicinal molecule pockets, according to Selvamuthukumar S et al. Pharmaceutics, biomedicine, cosmetics, bioremediation, water purification, catalysis, and agro-chemistry employ nanosponges to improve cyclodextrin performance [3].

In a plethora of recent publications, researchers have utilized a wide range of experimental and numerical methods to delve deeply into the molecular-level properties and structure of cyclodextrin nanosponges. In this compilation, you will find the following publications: Nanosponges have numerous applications and profiles, but a The reaction procedure is difficult to standardize because CD and cross-linker are randomly distributed, making synthesis problematic [4]. Using convective heating, ultrasound, and microwaves, Swaminathan et al and Anandam synthesized cyclodextrin nanosponges. Since discovery, convective heating has produced nanosponges. In dimethylformamide, butanone, pyridine, or dimethyl-sulfoxide, organic carbonate nanosponges need both reagents. This is an extremely hot process. Multiple organic molecule complexations can be seen to take place inside a reticulate structure when exposed to unregulated and non-uniform reaction conditions [5].

Considerable amounts of time, energy, pressure, reagents, catalyst, solvent, concentration, and pH are among the numerous factors that influence the yield, practical purity, and selectivity of any synthetic process. Algorithm optimization of process factors necessitates laborious investigation into the intricate interrelationships of the parameters. Because of this, the results obtained through conventional experimental analysis methods are useless [6-8]. Optimizing a chemical reaction means giving careful consideration to each and every one of the variables that might affect its outcome. Thus, this work set out to investigate and improve CDNS synthesis in pursuit of operational parameter optimization [9].

Statistical experimental designs make it possible to examine the impact of numerous variables simultaneously. Since experimental design is a systematic approach to consistently and effectively probe factor effects, using fewer trials than investigating one factor yields more relevant and trustworthy results. Experimentation and data analysis may identify crucial elements and relationships [10]. Experimental statistics has several chemical science applications.

When developing experimental designs with multiple interactive parameters, responding surface methodology (RSM) can be a useful statistical tool. Another application of RSM is in determining the optimal combination of components to elicit a desired reaction. Using fewer trials to evaluate specified variables on one another, RSM methods have long been used.

MATERIALS:

Bicalutamide were obtained as gift samples from Hetero Pvt. Ltd., Hyderabad, India, and were used without further purification. Hydroxypropyl β-cyclodextrin (HP-β-CD) and β-cyclodextrin (β-CD) were procured from Hi Media Laboratories Pvt. Ltd., Mumbai. Ethyl cellulose and polyvinyl alcohol (PVA) were purchased from Loba Chemie Pvt. Ltd., Mumbai. Analytical reagent (AR) grade solvents including dichloromethane, methanol, and ethanol were obtained from Loba Chemie Pvt. Ltd. and Merck Pvt. Ltd., Mumbai. Sodium hydroxide and hydrochloric acid of AR grade were supplied by Hi Media Laboratories Pvt. Ltd., Mumbai. Phosphate buffers were prepared using sodium dihydrogen orthophosphate (Hi Media Laboratories Pvt. Ltd., Mumbai) and potassium dihydrogen phosphate (Lab India, Mumbai).

Journal of Chemical and Pharmaceutical Sciences

Journal of Chemical and Pharmaceutical Sciences-JCHPS (2025) 18 (2): 67-81
Online ISSN: Online 2349-8552, Print ISSN: 0974-2115
Research Article | Pharmaceutical Sciences | MCI Approved | Peer-Reviewed | Refereed| OA Journal |

Carbopol 934 and triethanolamine were purchased from Meher Chemie, Mumbai. Surfactants including Tween 80 and Span 60 were obtained from M/s Alkem Laboratories Pvt. Ltd., Mumbai. A dialysis membrane (MWCO suitable for in vitro drug release studies) was procured from Hi Media Laboratories Pvt. Ltd., Mumbai. All other chemicals and reagents used were of analytical grade and used as received.

Development, Characterization of BCL-NS

Optimization of BCL-NS

A lot of work went into creating best NS for quality goal product profile Very important for product practicality. Therefore, it is an important step that must be highlighted for the end product to be believed to be safe, effective, and of high quality. Nevertheless, this cannot be achieved without giving careful thought to the CPPs and CMAs, which have the potential to influence the CQAs (critical quality attributes) [11-15]. Table 1 displays all of the QTPP's required components along with their validation for BCL-NS fabrication. Addressing the specific research goals of these QTPPs is crucial. Think about how you'll be using the product; its properties that are relevant to the skin should be perfect for that task. Ishikawa plot (Figure 1) provides more details regarding the development process's risks, necessary conditions, and CQA.

Table 1: QTPP & its rationale for making BCL-NS.

QTTP	Target	Justification
Drug Delivery system	Nanosponges	Compared to other nanosystems, it has improved oral retention.
Type of Dosage	Controlled Release	It improves drug absorption.
Administration route	Oral	Non-invasive, on-site medication administration, and simplicity of use are their advantages.
Drug release studies (%)	More than 85 %	Optimization of therapeutic and pharmacological action requires it.

β-CD NS Synthesis

Created a CD-based NS utilizing HP-ᵝ-CD and ᵝ-CD polymers, CDI, and dimethyl carbonate as cross-linking agents. Swaminathan et al. (22) has developed hot melt NS using varied polymer-crosslinker molar ratios. To summarize, the anhydrous polymer and the crosslinker were combined for several hours at temperatures approximately 90°C. Filtration was used to remove the solid byproduct from the reaction mixture after cooling. The next step was a light grinding to crumble the solid. To remove impurities and unreacted crosslinkers, we conducted a Soxhlet assembled extraction in ethanol. The NS was purified after the reaction with an excess of cross-linker and stored at 25°C until needed again [16].

NS drug loading

Over the course of 24 hours, we meticulously measured drug doses and magnetically stirred NS suspensions in water. Ten minutes at 2000 rpm removed colloidal supernatant from uncomplexed medication. Make antibiotic-loaded NS by freeze-drying colloidal supernatants in a Modulyo (Edwards, UK) freeze dryer. Room-temperature covered vacuum desiccator stored NS for future investigation [17, 18].

Fabrication of β-CD-NS

Various excipient amounts, such as β-CD (mol), crosslinker concentration (mol), and reaction time (h), were utilized in the emulsion diffusion method to create the NS. The continuous phase contained an adjustable surfactant concentration in a 20 mL water-based crosslinker solution, while the dispersed phase contained a 2 mL dichloromethane solution

Journal of Chemical and Pharmaceutical Sciences

Journal of Chemical and Pharmaceutical Sciences-JCHPS (2025) 18 (2): 67-81
Online ISSN: Online 2349-8552, Print ISSN: 0974-2115
Research Article | Pharmaceutical Sciences | MCI Approved | Peer-Reviewed | Refereed| OA Journal |

containing the optimal volume of polymer and both medications. Using the specified parameters (35 °C, 1000 rpm for 2 hours), the organic and water phases were mixed. After the NS was collected, there was a drying period of 24 hours at 40 °C [19].

A response surface model is shown using Design Expert®'s integrated data. Incomplete factorial algorithms with three levels produce BBDs of second order [20]. Improved NS synthesis was seen in the Box Behnken three-tiered study. Split into two flat parts and a single zero-set part. Using Stat-Ease Inc.'s Design Expert® (12.0.3.0, Minneapolis, MN, USA), we evaluated the second-order algebraic model's quadratic response surfaces. This optimization of BBD requires fifteen trials with three centers. Implicit models are described by quadratic equations, which include the following: duration of reaction (h), concentration of crosslinker (mol), and concentration of polymer. size of particles (Y1), EE, zeta strength (Y4), PDI (Y3), and optimisation were affected [21]. Table 2 compares the variable to the projected outcomes. Table 2 contains all of the components, both independent and dependent. Independent factors contribute to the additional data set. The model was defined by seventeen trials with three experimental levels and three factors altogether. Here are the outcomes [22].

We may summarize the variables The sequence b0, b1x1, b2x2, b3x3, b4x4, b12x1x2, b13x1x3, b23x2x3, b11x21, b22x22, and b33x23 are all integers.

Y represents the coded independent variables X1, X2, and X3, B0 is the intercept, and X2 is the measured response for each component match. Get the b1-b33 regression coefficients from experimental Y-values. The interaction and quadratic terms are XiXj because i and j might be 1, 2, or 3 [23]. Based on the low (−1), medium (0), and high (+1) values from the experiment, choose the polymer molar concentrations (X1), crosslinker concentrations (X2), and reaction time (X3). Three variables were measured: particle diameter, entrapment effectiveness, and profile depth index.

Table 2: Box-Behnken Design dependent as well as independent factors including levels and objectives

Parameter	Low (-1)	Medium (0)	High (+1)
Independent Variables			
A: Polymer concentration (mol)	1	2	3
B: Cross linker concentration (mol)	1	5.5	10
C: Reaction time (h)	1	2	3
Dependent variables			
Y1: Particle size (nm)	Minimize		
Y2: Polydispersity index	In range		
Y3: Entrapment efficiency	Maximize		

Based on the results, BBD is clearly the superior experimental design. All signs point to less work and time spent with three variables, twelve runs, and three center-point replicates. The analysis makes use of three main levels of coding for each component. To avoid potentially undesirable outcomes, experiments conducted under extremely high or low conditions are irrelevant [24]. Based on Table 13, we can deduce the dependent and independent variables

Checkpoint Analysis

By solving the related polynomial equations, we were able to discover the theoretical values of PDI, zeta potential, particle size, and entrapment efficiency. We took three points at random from each contour plot and used them as a control variable. At each of the three checkpoints, the theoretically obtained values were compared statistically to those of the experimentally prepared nanosponge formulation [25].

Journal of Chemical and Pharmaceutical Sciences-JCHPS (2025) 18 (2): 67-81
Online ISSN: Online 2349-8552, Print ISSN: 0974-2115
Research Article | Pharmaceutical Sciences | MCI Approved | Peer-Reviewed | Refereed| OA Journal |

We used multicriteria decision analysis (MCDA) to combine the two responses into a single composite response system, optimizing the NS entrapment efficiency and particle size simultaneously. To compensate for the drawbacks of unstructured decision-making, MCDA offers a methodical approach to selecting options using multiple criteria [26]. By utilizing the desirability function in Design-Expert® Version 9.0.6, the ideal NS formulation was derived. We can forecast the ideal point that stands for maximum desirability with the use of software optimization tools and the desirability criteria of response surface methodology. These tools identify which variables had an effect on each response and how large that effect was. The nature of the objective might change depending on how the points are weighted for each answer. The goal fields for each answer can take on one of five possible values: inside range, target, minimum, maximum, or none. Here is the next logical step after numerical optimization: graphical optimization. The factors' relationships with the response could be examined more thoroughly using overlay and desirability plots. In order to find the best formula, two parameters were considered: maximum entrapment and ideal particle size [27].

Formulation Optimization

Moreover, response surface plots [28] graphically demonstrated the impact of each variable on the responses. The software's overlay plot then used the specified goals and constraints to foretell the optimal nanosponge formulation formulas. Additional validation of the optimized formulae with desirability factors close to one was achieved by the use of a comparison between the software's projected response values and those produced experimentally.

Characterization of Prepared β-CD-NS

The optimized NS was characterized using a number of different processes. We used SEM, TEM, DSC, and XRPD. Productivity, particle size, entrapment, zinc potential, and PDI were among the other parameters assessed [29].

Particle characterization

UK-based Malvern Zetasizer Nano ZS measured particles. We tested BCL NS. Polystyrene cuvettes held 1:200 distilled water-diluted inquiry samples. We measured particle size and PDI using DLS. A cuvette was used to assess zeta potential and all other potentials. Every one of the three samples was examined three times [30].

Efficiency of entrapment (EE) along with drug loading

The dispersion filtrate was tested for drug loading (DL) and the efficiency of entrapment (EE) after 30 minutes of ultracentrifugation at 16,900 xg and 4 0C. For this purpose, we utilized the 5418R centrifuge, which is made by Eppendorf of Hamburg, Germany. The concentrations of BCL were measured using UV-visible spectroscopy at 234 and 270 nm, after filtering the supernatant. To calculate the EE and DL of BCL loaded NS, we employed the following equations [31].

$$\text{Entrapment efficiency (\%)} = \frac{\text{Initial amount of drug added-Drug amount in supernatant}}{\text{Initial amount of drug added}}$$

$$\text{Drug loading (\%)} = \frac{\text{Initial amount of drug added-Drug amount in supernatant}}{\text{Total amount weight of nanosponge}}$$

Size of the particles, PDI, potential of Zeta

In order to determine the zeta potential, particle size, and PDI of nanosponges, a Malvern Zetasizer (nano ZS, Malvern instruments Ltd., UK) used dynamic light scattering.To ensure accurate results, we used a clear, disposable zeta cell to

Journal of Chemical and Pharmaceutical Sciences-JCHPS (2025) 18 (2): 67-81
Online ISSN: Online 2349-8552, Print ISSN: 0974-2115
Research Article | Pharmaceutical Sciences | MCI Approved | Peer-Reviewed | Refereed| OA Journal |

thoroughly mix the samples with double distilled water before examination. To reduce the margin of error, we examined each sample three times and maintained the instrument temperature at 25 °C throughout [32].

Morphological Characterizations

Scanning electron microscopy (SEM)

A 40 kV/20 mA Goniometer Ultima IV X-ray diffractometer, equipped with an auto sampler, was used to record the XRD pattern of the constructed nanosponges. The samples were scanned using a continuous scanning type setup with a k-beta filter set at 3 and 50 degrees 2. To ensure that the medication had been adequately contained, we looked for changes in unusual peaks that did not conform to the usual drugspectra [33].

Release Studies In Vitro

Activated dialysis bags in a dissolving chamber were used to study DS, BCL-NS, and commercial BCL medication release. A system speed of 100 rpm and an operating temperature of 37 ± 0.5 °C were involved. For this purpose, we devised phosphate buffers with physiological pH 7.4 and intestinal pH 1.2. This allowed us to ascertain the release profile. If you want to keep the sink state going, just add 5 mL of new dissolving media to the reservoir every time. Purified and quantified at 210 nm. Applying many kinetic models to the data allowed us to determine the drug release mechanisms and their kinetics [34].

***In vivo* Pharmacokinetic Studies**

The pharmacokinetic study divided six male Sprague Dawley rats (n=6) into three groups at 8-10 weeks. In a specific order, the third group got BCL at mg/kg BW intravenously (iv). First and second groups received oral BCL-NS solutions. With LAC-2017-0282, Motherhood University met its requirements. After treatment, half a millilitre of blood was drawn at 5, 10, 45, 60, 120, 240, 480, 720, and 960 minutes. Blood samples were taken by spinning heparinization tubes at Rotate at 4000 rpm for 10 minutes at 4 °Cr. The liquid beyond the solid phase was frozen at -80 °C. was HPLC-UV analysed. Protocol for detecting BCL in rat plasma: Using this approach, a column thermostat at 30 °C, 5 µL sample injection, and 0.8 mL/min HPLC-UV at 268 nm were used. Considerations for this investigation included: 0.1 M acetate buffer and 10:1 methanol formed the mobile phase. Five nanolitres of hydrochloric acid were added to two liters of 16.4-gram sodium acetate buffer to correct the pH to 5.0. The PK parameters, including mean ± SD values for each treatment group, were analysed non-compartmentally. Calculated and displayed using standard deviations: When analysing the plasma drug concentration-time curve, the important variables to consider are the terminal elimination rate steady state (Ke), half-life (T1/2), AUC0-last, and AUC0→∝. Section of a curve split. (AUC0→∞) for by the BCL AUC0→∞ to get the metabolic ratios for BCL.

Analysis of statistical Data

Unless otherwise specified, reports are shown as the average augmented or diminished by the dispersion of the data significance level in one-way analyses of variance or p-values below 0.01, which signified the t-tests.

RESULTS AND DISCUSSION

Optimization of BCL-NS

A primary goal was to enhance the skin retentivity of BCL-NS. To maximize the therapeutic effect of a high-quality, patient-centered formulation, the QTPP has to be prepared in advance. In order to determine CQA, the improved systems

Journal of Chemical and Pharmaceutical Sciences-JCHPS (2025) 18 (2): 67-81
Online ISSN: Online 2349-8552, Print ISSN: 0974-2115
Research Article | Pharmaceutical Sciences | MCI Approved | Peer-Reviewed | Refereed| OA Journal |

were selected, which include study variables. Each affects vesicle size (Y1), PDI (Y3), reaction time (C), zetapotential (Y1), entrapment efficiency (Y2), polymer concentration (A), and crosslinker (B The coefficients illustrate how A, B, and C impact Y1, Y2, and Y3. Higher-order terms are interaction terms, whereas Fourier coefficients are quadratic correlations. Positive signs signify cooperation, whereas negative signals indicate conflict. Backward elimination made the quadratic model fit data. Tables 3 of the ANOVA analysis show statistical significance ($P \leq 0.014$) for all polynomial equations using design expert software. The vesicle size (Y1) mathematical model has an R2 value of 0.9892 and an F-value of 70.95 ($p \leq 0.0001$). Size of the vesicle is greatly affected by A, B, and C, as well as the quadratic factors AB, AC, and BC (Table 3). With p-values more than 0.05, not a single feature was considered significant. The results show that A is more powerful than B and C. Counter and 3D response surface graphs indicate independent parameters' main and interaction particle size effects.

Table 3: Design layout and responses noted for BCL-NS formulations

Std	Run	A	B	C	Y1	Y2	Y3	ZP
1	15	1	1	2	240.35±2.35	71.12±0.05	0.362±0.91	-17.37±1.14
2	9	3	1	2	369.28±3.14	54.37±0.09	0.243±0.16	-21.68±1.31
3	8	1	10	2	253.17±1.26	48.72±0.01	0.423±0.28	-23.35±1.12
4	1	3	10	2	470.12±3.25	62.53±1.05	0.511±0.17	-25.09±1.26
5	14	1	5.5	1	176.35±2.06	82.49±0.36	0.273±0.43	-28.34±1.12
6	10	3	5.5	1	520.31±2.31	65.05±0.13	0.382±0.09	-26.05±1.52
7	4	1	5.5	3	506.29±1.45	54.37±1.24	0.552±0.06	-27.58±1.45
8	6	3	5.5	3	405.76±5.26	67.94±2.05	0.243±0.07	-21.46±1.37
9	13	2	1	1	163.25±3.27	76.24±2.18	0.351±0.02	-31.16±1.19
10	2	2	10	1	320.98±1.52	75.34±3.09	0.299±0.08	-25.57±1.24
11	12	2	1	3	365.42±2.04	72.69±0.51	0.197±0.14	-27.59±1.06
12	7	2	10	3	349.86±2.06	58.02±0.67	0.482±0.01	-29.84±1.15
13	11	2	5.5	2	284.36±3.08	76.35±0.15	0.158±0.06	-34.45±1.28
14	16	2	5.5	2	275.49±2.51	74.96±0.56	0.172±0.09	-27.41±1.26
15	17	2	5.5	2	254.38±3.06	75.34±0.32	0.142±0.08	-30.59±1.14
16	5	2	5.5	2	287.92±3.45	84.69±0.14	0.143±0.04	-28.59±1.02
17	3	2	5.5	2	280.61±2.74	73.34±0.33	0.139±0.02	-29.49±1.31

Significance of Model F-value 63.02. F-values over 0.01% may suggest random chance. The P-values for the model's key terms are less than 0.0500. Some examples of common words are: A, B, C, AB, AC, BC, A^3, B^3, C^3. As soon as there are more than 0.1001 superfluous model words. An F-value of 2.75 Comparing Lack of Fit to simple mistake makes it seem insignificant. 17.63% loud F-values misbehave.

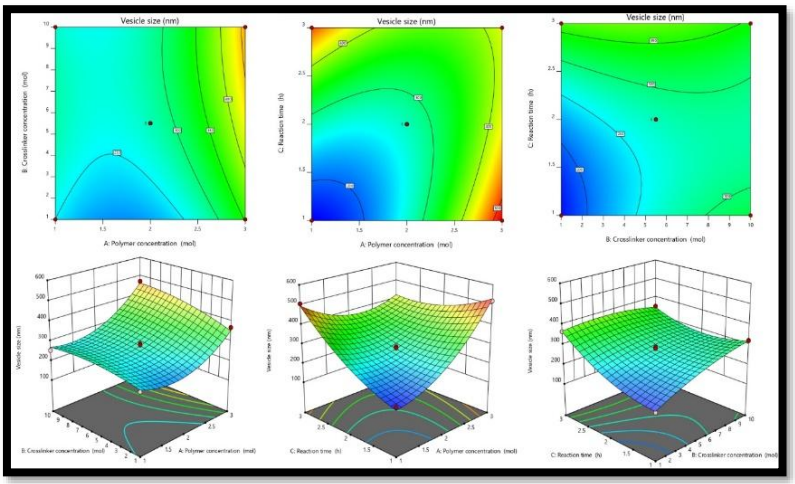

Figure 1: 3D response surface and contour plot for vesicle size

Journal of Chemical and Pharmaceutical Sciences

Journal of Chemical and Pharmaceutical Sciences-JCHPS (2025) 18 (2): 67-81
Online ISSN: Online 2349-8552, Print ISSN: 0974-2115
Research Article | Pharmaceutical Sciences | MCI Approved | Peer-Reviewed | Refereed| OA Journal |

Predicted R^2= 0.8624 and Adjusted R^2= 0.9721 are almost same, as evaluated by Adeq Precision, with a Signal-to-Noise Ratio (SNR) below 0.2. Above 4 is the ideal ratio. Confirmed 27.536 ratios. Consider using this paradigm to browse design.

Size of vesicle: +276.55 +73.66A +31.98B +55.81C +22.01AB -111.12ABC -43.32BC +79.49A2 -22.81B2 +46.

The experiment perturbation map (Fig. 1) shows how A, B, and C impact nanoparticle vesicle size (Y1). A affects Y1 most, followed by B somewhat and C none.

Figure 2 shows the response surface plots for a given value of C, which may help us comprehend the link between the two sets of variables. It shows the relationship between A and B with respect to vesicle size (Y1), for example. At low A values, Y1 becomes visible when the polymer concentration is raised from 240.35±2.35 nm to 506.29±1.45 nm. An increase in Y1 from 254.38±3.06 nm to 405.76±5.26 nm is also seen at high A levels. Table 2 shows that the nanosponge vesicle sizes varied from 284.36±3.08 to 470.12±3.25 nm. Factorial of particle size has a statistically significant F-value of 70.95 and correlation coefficient of 1.000. If "Prob 4 F" is less than 0.0500, model terms are relevant.

Coded factors allow the equation to predict component outcomes. Normal level 1 factors are +1. Whereas the notation for level -1 factors is -1. To see how the elements stack up against one another, you may use the coded equation to compare their coefficients.

The 62.19 F-value suggests model relevance. 0.01% sheer chance generating a high F-value is implausible. A significant model term p-value is < 0.0500. The key model terms are A^3, B^3, BC, AB, and AC. Model terms over 0.1000 are irrelevant. The model may be improved by removing unnecessary sentences (excluding hierarchy keywords). Lack of Fit has little statistical significance compared to pure error (F=0.27). A high Lack of Fit F-value (84.35 percent chance) is probably just noise.

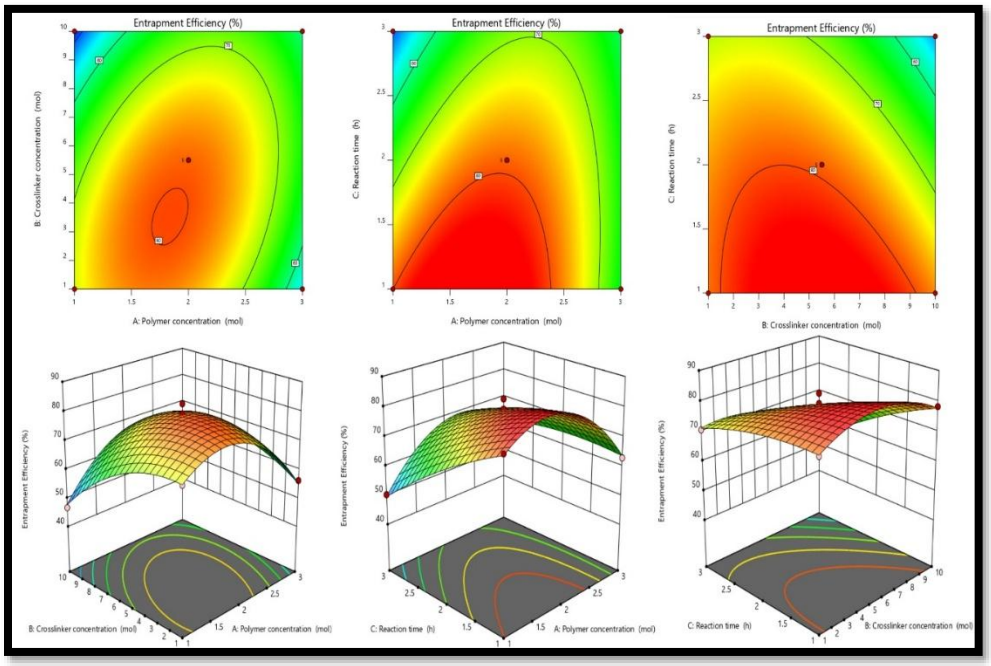

Figure 2: 3D response surface and contour plot for Entrapment Efficiency

Journal of Chemical and Pharmaceutical Sciences-JCHPS (2025) 18 (2): 67-81
Online ISSN: Online 2349-8552, Print ISSN: 0974-2115
Research Article | Pharmaceutical Sciences | MCI Approved | Peer-Reviewed | Refereed| OA Journal |

The expected R^2 value of 0.9505 and the adjusted R^2 value of 0.9718 are quite close to each other, differing by less than 0.2. Checking the signal-to-noise ratio is what Adeq Precision really does. Above 4 ratios are best. Signal-to-noise ratio should be 20.893. This model traverses design. Efficient entrapment: A = 79.14, -1.10A, -4.85B, -8.14C, +7.39AC, -4.44BC, -13.28A2, -6.92B2, -2.14C2.

Using coded factors, the equation may predict output for certain element values. High and low levels default to +1& -1. Coefficient comparisons utilizing the coded equation could help us determine which parts are more important.

A 31.66 F-value indicates model significance. A high F-value's 0.01% probability implies a coincidence. With a p-value below 0.0500, we can say that this model component is significant. Within this model, significant variables are $A_{\circ}$, Bɲ, Cɲ, AB, AC, BC, and A^3. A value of 0.1000 causes the model terms to be disregarded. If you want to make your model better, try removing terms that don't have a hierarchy. Considering the significance of pure error, an F-value of 0.41 for lack of fit is negligible. For 75.45 percent of instances, this Lack of Fit F-value could be due to noise. Any little discrepancy is tolerable as a perfect fit with the model is desirable.

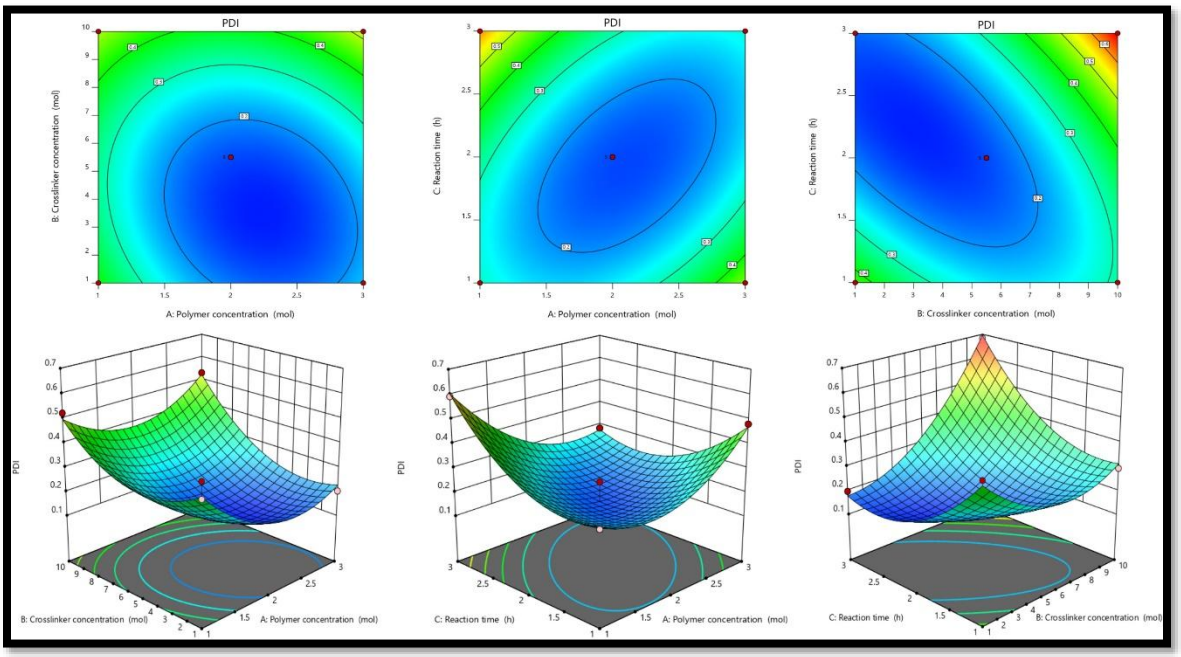

Figure 3: 3D response surface and contour plot for PDI

Consider model relevance with F=31.66. The 0.01% high F-value probability is a coincidence. Model terms that are considered significant have less than 0.0500 for the p-values. The primary variables in this model are $A_{\circ}$, BЎ, Cɲ, AB, AC, BC, and A^3. The predictive terms are disregarded when the value falls below 0.10000. If at all possible, avoid using phrases that do not indicate hierarchy in your model. The discordance is negligible when weighed against the uncertainty, with an F-value of just 0.41. In 75.45% of cases, this F-value for Lack of Fit might just be noise. A ratio greater than 4 is considered optimal. You have an adequate signal with a ratio of 16.793. Using this paradigm is one approach to navigating the design space.

Here is the formula for the PDI, or present value of the integral: The equation is (0.1602 -0.0364A +0.0984B +0.0305C +0.0492AB -0.1270AC +0.1605BC +0.1280A2 +0.1240B2 +0.1218C2).

Journal of Chemical and Pharmaceutical Sciences-JCHPS (2025) 18 (2): 67-81
Online ISSN: Online 2349-8552, Print ISSN: 0974-2115
Research Article | Pharmaceutical Sciences | MCI Approved | Peer-Reviewed | Refereed| OA Journal |

Use the coded factor equation to predict any component level. In level 1, factors are generally +1. Whereas the notation for level -1 factors is -1. To see how the elements stack up against one another, you may use the coded equation to compare their coefficients.

Optimization

We looked at the independent variable optimization using the desirability method. Numerical optimization found the best independent variables (A, B, and C) to maximize response variables (Y1, Y2, and Y3) within given limitations. Design-Expert® discovered independent variable restrictions and made three formula changes. Table 4 shows expected and actual medication entrapment efficiency (Y2), particle size (Y1), and PDI (Y3). Data analysis showed these variables predicted and actual values were similar. Accordingly with results, formulation F5 is the best BCL-scaffold polymeric nanoparticle formulation, and the optimization strategy was successful, as the expected and actual values were quite close to each other [72].

Table 4: Check point analysis for optimized BCL-NS formulation (F5)

F5	A	B	C	Y1	Y2	Y3	Desirability
Predicted	1.409	2.731	1.331	161.999	83.624	0.281	0.982
Observed	1	5.5	1	176.35±2.06	82.49±0.36	0.273±0.43	
Relative Error	-0.049	2.769	-0.331	14.351	-3.134	0.002	

Size of Particles, PDI, Potential of zeta

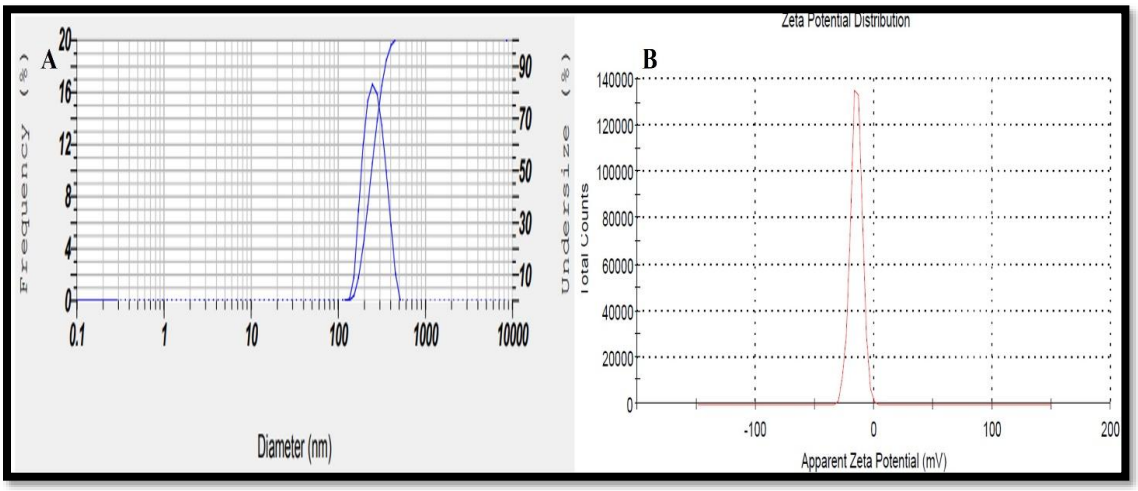

Figure 4: Determination on A) distribution in size of the Particle, B) Apparent zeta potential

Morphological Surface studies:

Optimised BCL-NS surface morphology was assessed using SEM and TEM. Figure 1A shows that particles agglomerate and are porous, supporting the earlier work reporting the porous structure of optimized BCL-NS (Varan et al., 2020). The possibility that arabinoxylan is a factor in the aggregation was discovered by De Anda-Flores et al. (2020). A photomicrograph of the optimized BCL-NS was shown in Figure with a 200 nm scale bar. The resultant nano-form was round and had a smooth surface. Previous research supported similar conclusions (Kumar and Rao, 2021) that drug loading had no effect on the spherical form of β-CD-based NS. According to Kumar et al. (2018), another study also documented the existence of a morphologically spherical γ-CD-NS encapsulating crosslinker.

Journal of Chemical and Pharmaceutical Sciences-JCHPS (2025) 18 (2): 67-81
Online ISSN: Online 2349-8552, Print ISSN: 0974-2115
Research Article | Pharmaceutical Sciences | MCI Approved | Peer-Reviewed | Refereed| OA Journal |

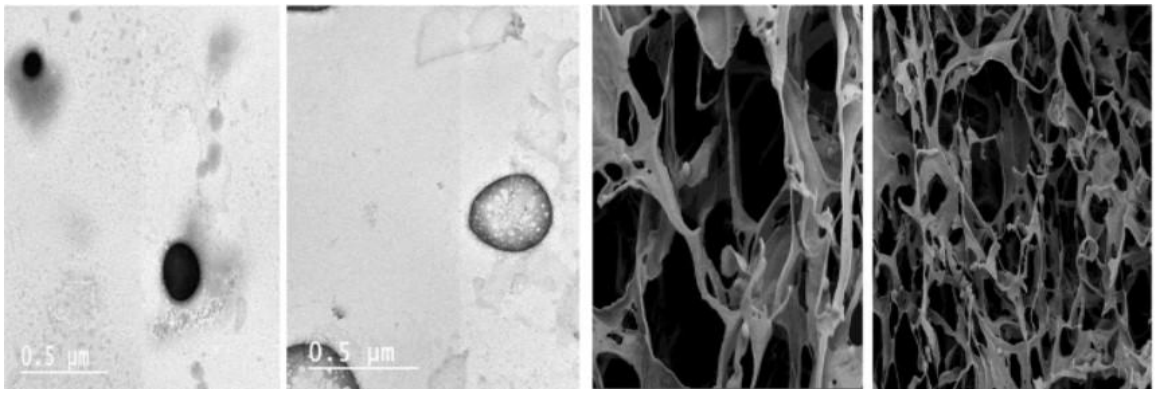

Figure 5: Nano sponge improved formulations (F5) TEM and SEM micrographs.

Drug release examination invitro

Because BCL-NS dissolution is decreasing, recrystallization of BCL could be the cause. In Figure 10, you can see the mean dissolution profile of BCL as well as the selected ternary SDS. Its limited aqueous solubility in 0.1N HCl with 1% SLS causes pure BCL to dissolve slowly. BCL's amorphous form in the spray-dried ternary SD (T-004) increases its dissolving rate in 0.1N HCl with 1% SLS. The presence of POL in the SD is also responsible for the initial burst effect in the dissolution, according to Kundu (2022).

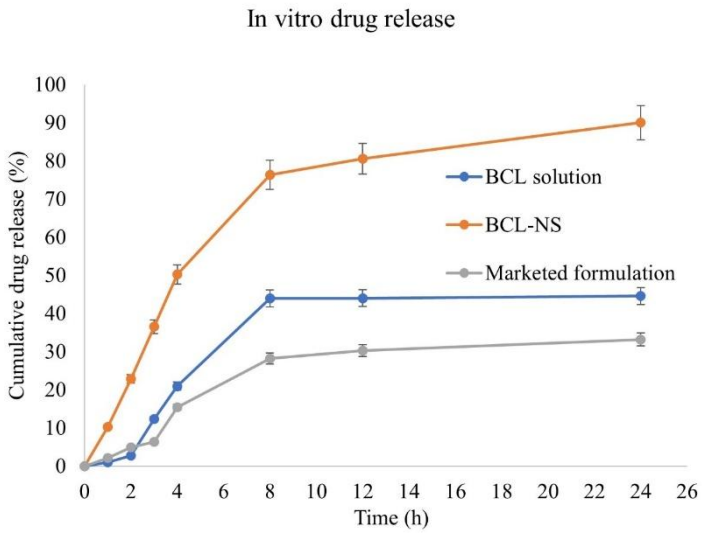

Figure 6: Optimized BCL-NS formulation (F5) in-vitro release examination

Looking at Fig. 1B, we can see that after 2 hours, the marketed formulation had a cumulative release percentage of 2.76%, while after 8 hours, it was 43.97% and 28.23%, and after 24 hours, it was 44.57% and 33.22%. Contrarily, NS that were loaded with drugs showed BCL concentrations of 22.88% after 2 hours, 76.32% after 8 hours, and 90.04% after 24 hours. Experimental results showed that the NS sped up the rate of drug dissolution from the nanoemulsion for both drugs. First-order kinetics described NS drug release effectively. This model best depicted release with the greatest BCL correlation value (R2; 0.9517). Higuchi found a link with BCL (0.8688), while the zero-order release model did not (R2; 0.7363). BCL correlation coefficients were Hixon-Crowell (0.9352) and Korsmeyer-Peppas (0.8925, n; 0.40).

Journal of Chemical and Pharmaceutical Sciences-JCHPS (2025) 18 (2): 67-81
Online ISSN: Online 2349-8552, Print ISSN: 0974-2115
Research Article | Pharmaceutical Sciences | MCI Approved | Peer-Reviewed | Refereed| OA Journal |

Pharmacokinetic studies

Table 5: Pharmacokinetic parameters of BCL and optimized BCL-NS after administering in rats intravenously.

Parameters	BCL Solution	BCL-NS	BCL-IV
Intercept	2.755102	3.085738	3.233275
Slope	-0.02384	0.005559	-0.03874
C0 (mcg/mL)	568.9859	1218.256	1711.098
k (h-1)	0.054908	-0.0128	3.233275
dose (mg)	50	50	-0.03874
dose (mcg)	50000	50000	1711.098
vd (mL)	87.87564	41.04229	0.089207
Vd (L)	0.087876	0.041042	10
$t_{1/2}$ (h)	12.62112	-54.1292	10000
Clearance (l/h)	4.393782	2.052115	5.844201
AUC $_{0-t}$ (µg.h/mL)	0.041618	0.03654	0.005844
AUC $_{1-t}$ (µg.h/mL)	8572.478	80334.46	7.768424
AUC1-inft (µg.h/mL)	190.6828	114292	0.058442
AUC $_{tot}$ (µg.h/mL)	8763.202	33957.8	0.044191
C_{max} (µg/mL)	5890.12	8823.16	4536.29
T_{max} (h)	1.02	36.92	5.69
MRT (h)	4.13	40.26	4.29

BCL-NS' oral pharmacokinetics in male SD rats indicated its live animal potential. Concentration-temperature plasma curves. Table 4 contrasts noncompartmental plasma concentration-time patterns [22]. NS boosts BCL pharmacokinetics. The BCL AUC was substantially higher in the NS formulation (h ng mL− 1) compared to the aqueous solution ($p < 0.05$ The BCL-NS AUC0-t was 80334.46 and 7.768424. Compared to the aqueous solution, the NS formulation had higher Cmax (ng mL− 1) for BCL and commercialized formulation (8823.16 and 4536.29, respectively The t1/2 of oral BCL-NS and aqueous solution was shorter than the commercial formulation.

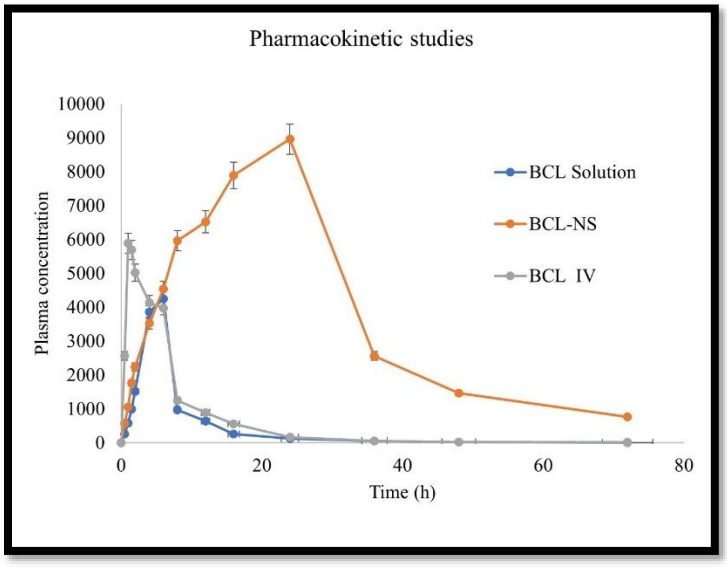

Figure 7: BCL-NS at 50 mg/kg orally vs. BCL aqueous suspension in male SD rats.

CONCLUSION:

Using a Box-Behnken Design (BBD) technique inside the Quality by Design (QbD) framework, the current study proved that BCL-NS, nano sponges loaded with β-cyclodextrin, can be effectively formulated and optimized. The optimized nano sponge had good physicochemical features, such as a stable and uniform structure, a low polydispersity index (0.273 ± 0.43), and a particle size of 176.35 ± 2.06 nm. It also had high entrapment efficiency (82.49 ± 0.36%). The in-vitro drug release profile showed a steady release pattern, with a cumulative release of over 90% after 24 hours. It also followed first-order kinetics, which means that the drug release is reliant on the concentration. The spherical and porous shapes were validated by surface morphology tests (SEM and TEM), which are ideal for regulated drug delivery. The nano sponge system was found to be superior to standard BCL formulations in the rat pharmacokinetic study, which also showed improved mean residence time (MRT), longer half-life, greater Cmax, and enhanced oral bioavailability. When it comes to treating prostate cancer, the newly created BCL-NS nanocarrier shows great promise as a long-acting oral delivery system for BCL. Therapeutic results, dose frequency, and patient compliance can all be improved with this nanotechnology-driven strategy. To back up clinical translation, future research must concentrate on evaluating anticancer activity and safety in living organisms.

REFERENCES:

1. Ferlay, J., Soerjomataram, I., Dikshit, R., Eser, S., Mathers, C., Rebelo, M., Parkin, D. M., Forman, D., & Bray, F. (2015). Cancer incidence and mortality worldwide: sources, methods and major patterns in GLOBOCAN 2012. International Journal of Cancer, 136, E359–E386.
2. Dieci, M. V., Arnedos, M., Delaloge, S., & Andre, F. (2013). Quantification of residual risk of relapse in breast cancer patients optimally treated. The Breast, 22(Suppl 2), S92–S95.
3. Myers, E. R., Moorman, P., Gierisch, J. M., Havrilesky, L. J., Grimm, L. J., Ghate, S., et al. (2015). Benefits and harms of breast cancer screening: A systematic review. JAMA, 314, 1615–1634.
4. Siegel, R. L., Miller, K. D., & Jemal, A. (2017). Cancer statistics, 2017. CA: A Cancer Journal for Clinicians, 67, 7–30.
5. Aggarwal, S., Verma, S. S., Aggarwal, S., & Gupta, S. C. (2021). Drug repurposing for breast cancer therapy: Old weapon for new battle. Seminars in Cancer Biology, 68, 8–20.
6. Hanahan, D., & Weinberg, R. A. (2011). Hallmarks of cancer: The next generation. Cell, 144, 646–674.
7. Barkat, H. A., Das, S. S., Barkat, M. A., Beg, S., & Hadi, H. A. (2020). Selective targeting of cancer signaling pathways with nanomedicines: Challenges and progress. Future Oncology, 16, 2959–2979.
8. Corona, S. P., & Generali, D. (2018). Abemaciclib: A CDK4/6 inhibitor for the treatment of HR+/HER2- advanced breast cancer. Drug Design, Development and Therapy, 12, 321–330.
9. The Cancer Genome Atlas Network. (2012). Comprehensive molecular portraits of human breast tumours. Nature, 490, 61–70.
10. Peurala, E., Koivunen, P., Haapasaari, K. M., Bloigu, R., & Jukkola-Vuorinen, A. (2013). The prognostic significance and value of cyclin D1, CDK4 and p16 in human breast cancer. Breast Cancer Research, 15, R5.
11. Gallorini, M., Cataldi, A., & Di Giacomo, V. (2012). Cyclin-dependent kinase modulators and cancer therapy. BioDrugs, 26, 377–391.
12. Jessen, B. A., Lee, L., Koudriakova, T., Haines, M., Lundgren, K., Price, S., et al. (2007). Peripheral white blood cell toxicity induced by broad spectrum cyclin-dependent kinase inhibitors. Journal of Applied Toxicology, 27, 133–142.
13. Fornier, M. N., Rathkopf, D., Shah, M., Patil, S., O'Reilly, E., Tse, A. N., et al. (2007). Phase I dose-finding study of weekly docetaxel followed by flavopiridol for patients with advanced solid tumors. Clinical Cancer Research, 13, 5841–5846.
14. Mita, M. M., Joy, A. A., Mita, A., Sankhala, K., Jou, Y. M., Zhang, D., et al. (2014). Randomized phase II trial of the cyclin-dependent kinase inhibitor dinaciclib (MK-7965) versus capecitabine in patients with advanced breast cancer. Clinical Breast Cancer, 14, 169–176.
15. Nemunaitis, J. J., Small, K. A., Kirschmeier, P., Zhang, D., Zhu, Y., Jou, Y. M., et al. (2013). A first-in-human, phase 1, dose-escalation study of dinaciclib, a novel cyclin-dependent kinase inhibitor, administered weekly in subjects with advanced malignancies. Journal of Translational Medicine, 11, 259.
16. Das, S. S., Alkahtani, S., Bharadwaj, P., Ansari, M. T., Md, F. A. L., Pang, Z., et al. (2020). Molecular insights and novel approaches for targeting tumor metastasis. International Journal of Pharmaceutics, 585, 119556.

17. Finn, R. S., Dering, J., Conklin, D., Kalous, O., Cohen, D. J., Desai, A. J., et al. (2009). PD 0332991, a selective cyclin D kinase 4/6 inhibitor, preferentially inhibits proliferation of luminal estrogen receptor-positive human breast cancer cell lines in vitro. Breast Cancer Research, 11, R77.
18. Fry, D. W., Harvey, P. J., Keller, P. R., Elliott, W. L., Meade, M., Trachet, E., et al. (2004). Specific inhibition of cyclin-dependent kinase 4/6 by PD 0332991 and associated anti-tumor activity in human tumor xenografts. Molecular Cancer Therapeutics, 3, 1427–1438.
19. Toogood, P. L., Harvey, P. J., Repine, J. T., Sheehan, D. J., VanderWel, S. N., Zhou, H., et al. (2005). Discovery of a potent and selective inhibitor of cyclin dependent kinase 4/6. Journal of Medicinal Chemistry, 48, 2388–2406.
20. Gelbert, L. M., Cai, S., Lin, X., Sanchez-Martinez, C., Del Prado, M., Lallena, M. J., et al. (2014). Preclinical characterization of the CDK4/6 inhibitor LY2835219: In-vivo cell cycle-dependent/independent anti-tumor activities alone/in combination with gemcitabine. Investigational New Drugs, 32, 825–837.Rader, J., Russell, M.R., Hart, L.S., Nakazawa, M.S., Belcastro, L.T., Martinez, D., Li, Y., Carpenter, E.L., Attiyeh, E.F., Diskin, S.J., Kim, S., Parasuraman, S., Caponigro, G., Schnepp, R.W., Wood, A.C., Pawel, B., Cole, K.A., Maris, J.M., 2013. Dual CDK4/ CDK6 inhibition induces cell-cycle arrest and senescence in neuroblastoma. Clin. Cancer Res. 19, 6173–6182.
21. Rader, J., Russell, M. R., Hart, L. S., Nakazawa, M. S., Belcastro, L. T., Martinez, D., et al. (2013). Dual CDK4/CDK6 inhibition induces cell-cycle arrest and senescence in neuroblastoma. Clinical Cancer Research, 19, 6173–6182.
22. Tate, S. C., Cai, S., Ajamie, R. T., Burke, T., Beckmann, R. P., Chan, E. M., et al. (2014). Semi-mechanistic pharmacokinetic/pharmacodynamic modeling of the anti-tumor activity of LY2835219, a new cyclin-dependent kinase 4/6 inhibitor, in mice bearing human tumor xenografts. Clinical Cancer Research, 20, 3763–3774.
23. Asghar, U., Witkiewicz, A. K., Turner, N. C., & Knudsen, E. S. (2015). The history and future of targeting cyclin-dependent kinases in cancer therapy. Nature Reviews Drug Discovery, 14, 130–146.
24. Fernandes, M. T., Adashek, J. J., Barreto, C. M. N., Spinosa, A. C. B., de Souza Gutierres, B., Lopes, G., et al. (2018). A paradigm shift for the treatment of hormone receptor-positive, human epidermal growth factor receptor 2 negative (HR+/HER2−) advanced breast cancer: A review of CDK inhibitors. Drugs in Context, 7, 212555.
25. Dickson, M. A. (2014). Molecular pathways: CDK4 inhibitors for cancer therapy. Clinical Cancer Research, 20, 3379–3383.
26. Tripathy, D., Bardia, A., & Sellers, W. R. (2017). Ribociclib (LEE011): Mechanism of action and clinical impact of this selective cyclin-dependent kinase 4/6 inhibitor in various solid tumors. Clinical Cancer Research, 23(13), 3251–3262.
27. Lallena, M. J., Boehnke, K., Torres, R., Hermoso, A., Amat, J., Calsina, B., et al. (2015). Abstract 3101: In-vitro characterization of Abemaciclib pharmacology in ER+ breast cancer cell lines. Molecular and Cellular Biology, 3101.
28. Aiassa, V., Garnero, C., Longhi, M. R., & Zoppi, A. (2021). Cyclodextrin multicomponent complexes: Pharmaceutical applications. Pharmaceutics, 13(7), 1099.
29. Mane, P. T., Wakure, B. S., & Wakte, P. S. (2021). Cyclodextrin based nanosponges: A multidimensional drug delivery system and its biomedical applications. Current Drug Delivery, 18(10), 1467–1493.
30. Sherje, A. P., Dravyakar, B. R., Kadam, D., & Jadhav, M. (2017). Cyclodextrin-based nanosponges: A critical review. Carbohydrate Polymers, 173, 37–49.
31. Iravani, S., & Varma, R. S. (2022). Nanosponges for water treatment: Progress and challenges. Applied Sciences, 12(9), 4182.
32. Lembo, V., Folini, D., Wild, M., & Lionello, P. (2019). Inter-hemispheric differences in energy budgets and cross-equatorial transport anomalies during the 20th century. Climate Dynamics, 53(1), 115–135.
33. Almutairy, B. K., Alshetaili, A., Alali, A. S., Ahmed, M. M., Anwer, M. K., & Aboudzadeh, M. A. (2021). Design of Olmesartan Medoxomil-loaded NSs for hypertension and lung cancer treatments. Polymers, 13(14), 2272.
34. Ahmed, M. M., Fatima, F., Anwer, M. K., Ansari, M. J., Das, S. S., & Alshahrani, S. M. (2020). Development and characterization of ethyl cellulose NSs for sustained release of brigatinib for the treatment of non-small cell lung cancer. Journal of Polymer Engineering, 40, 823–832.
35. Sameina, L. H., Idamakantia, S., Chettupalli, A. K., Velamala, R. R., & Ezzat, M. O. (2023). Design of mesalamine loaded micro-particles: Preparation, in vitro and in vivo characterization. Materials Today: Proceedings, July 26.
36. Chettupalli, A. K., Avula, P. R., & Chauhan, V. (2024). Improved transdermal delivery of anti-hypertensive drug loaded nanostructured lipid carriers: Statistical design, optimization, depiction and pharmacokinetic assessment. Current Drug Therapy, 19(7), 828–845.
37. Chettupalli, A. K., Katta, S., Fateh, M. V., Haque, M. A., Kothapally, D., Damarasingu, P., et al. (2025). Design, optimization, and characterization of zolmitriptan loaded liposomal gels for intranasal delivery for acute migraine therapy. Intelligent Pharmacy, 3(1), 11–25.
38. Chettupalli, A. K., Unnisa, A., Peddapalli, H., Jadi, R. K., Anusha, K., & Amarachinta, P. R. (2025). Development and evaluation of empagliflozin-loaded solid lipid nanoparticles: Pharmacokinetics and pharmacodynamics for oral delivery. Intelligent Pharmacy, January 12.

39. Chettupalli, A. K., Kar, N. R., Iswariya, V. T., Panigrahy, U. P., Singh, L. P., Roy, H., et al. (2025). Development and optimization of dapagliflozin oral nano-bilosomes using response surface method: In vitro evaluation, in vivo evaluation. Nanotheranostics, 9(1), 1.
40. Chettupalli, A. K., Bukke, S. P., Udom, G. J., Saraswathi, T. S., Rahaman, S. A., Rai, S. N., et al. (2024). Investigating new bilosomes for ex vivo skin deposition, in vitro characterization, and transdermal delivery of nimodipine. Nanoscale Advances.
41. Chettupalli, A. K., Chokkarapu, S., Singh, A., Babu, M. R., Singh, M. P., & Bukke, S. P. (2025). Development and fabrication of a novel nano-bilosomal system for enhanced oral delivery of Trametinib: Apoptotic induction and anticancer efficacy evaluation. Materials Technology, 40(1), 2495346.
42. Chettupalli, A. K., Kakkerla, A., Jadi, R. K., Uppu, P., Ghazwani, M., Hani, U., et al. (2025). Design, development, and preclinical evaluation of pirfenidone-loaded nanostructured lipid carriers for pulmonary delivery. Scientific Reports, 15(1), 11390.
43. Marati, K., Palatheeya, S., & Chettupalli, A. K., Naik, Bukke, S. P. (2025). Characterization and interactions between piperine and ezetimibe in their anti-hyperlipidemic efficacy using biopharmaceutics and pharmacokinetics. BMC Pharmacology and Toxicology, 26(1), 7.
44. Chettupalli, A. K., Bukke, S. P., Rahaman, S. A., Unnisa, A., Adepu, M., Kavitha, M., et al. (2025). Ritonavir loaded solid lipid nanoparticles for oral drug delivery and bioavailability enhancement. Discover Applied Sciences, 7(1), 58.
45. Chettupalli, A., Amarachinta, P. R., Kuchukuntla, M. R., Katta, S., Vobenaboina, V. K., Garige, B. S., et al. (2025). Quality by design and characterization of nimodipine novel carriers for the treatment of hypertension: Assessment of the pharmacokinetic profile. Current Bioactive Compounds, 21(1), E230224227376.
46. Bukke, S. P., Mishra, S., Thalluri, C., Reddy, C. S., Chettupalli, A. K., & Kumar, G. A. (2024). Transformative approaches in bone pathology treatment: The efficacy of alendronate-infused hydroxyapatite microspheres. Journal of Biochemical Technology, 15(4), 9–16.
47. Priya, S. S., & Choudhury, A. (2023). Efficacy of metallic nanoparticles and nanocarriers as an advanced tool for imaging and diagnosis: Insight into theranostic applications. International Journal of Biomedical Investigation, 6, 149. https://doi.org/10.31531/2581-4745.1000149